METEOROLOGICAL APPLICATIONS
Meteorol. Appl. **18**: 188–197 (2011)
Published online 17 August 2010 in Wiley Online Library
(wileyonlinelibrary.com) DOI: 10.1002/met.228

RMetS
Royal Meteorological Society

The use of lidar-detected smoke puff evolution for dispersion calculations

A. Choukulkar,[a]* R. Calhoun[a] and H. J. S. Fernando[b]

[a] *Environmental Remote Sensing Group, Arizona State University, Tempe Campus, PO Box 876106, Tempe, AZ 85287-6106, USA*
[b] *Mechanical and Aerospace Engineering, Arizona State University, Tempe Campus, PO Box 876106, Tempe, AZ 85287-6106, USA*

ABSTRACT: Dispersion modelling is a key component of modern emergency responses to catastrophic atmospheric releases. However, periodic algorithmic advances are needed to effectively use new datasets acquired with modern remote sensing instruments. This work demonstrates that coherent Doppler lidar can be used to provide valuable new inputs for dispersion models. While related research seeks to retrieve other required inputs for dispersion modelling systems, for example velocity vectors from radial velocities, this paper assembles and contextualizes analytical and algorithmic approaches for an improved understanding of dispersion characteristics in specific atmospheric scenarios using Doppler lidar data. Longitudinal (along-wind), lateral (cross-wind), and vertical dispersion parameters are calculated and used to estimate eddy diffusivities based on Gaussian curve fitting and first-order closure. Empirical relations based on similarity theory are used to verify these estimates, and reasonable agreement is found between the two approaches. Several improvements are also suggested for the lidar scanning techniques to facilitate retrieval of dispersion parameters. Copyright © 2010 Royal Meteorological Society

KEY WORDS eddy diffusivity; remote sensing; emergency response; Doppler lidar; Gaussian model; JU 2003

Received 26 March 2010; Revised 2 July 2010; Accepted 6 July 2010

1. Introduction

Concern over the effects of daily pollution exposures and possible catastrophic releases of hazardous materials drives a growing interest for better understanding of dispersion in urban environments (Britter and Hanna, 2003). Atmospheric dispersion modelling has been a central component of previous urban studies (e.g. Hanna *et al*., 1982; Hanna and Paine, 1989) including those performed in the homeland security context (Van Aalst, 1990). Lidar has been used to measure plume shape, size and trajectory over time (e.g. Misra and McMillan, 1980; Savov *et al*., 2002) including measurements of variables such as mixed layer height, turbulence, friction velocity and dissipation which are important for dispersion studies (for example, Collier *et al*., 2005). However, relatively few studies (e.g. Hanna and Franzese, 2000; Min *et al*., 2002) have focused on the dispersion of puffs in the urban boundary layer.

Traditional methods used for dispersion studies involve the use of gas samplers placed in the mean wind direction, allowing the indirect estimation of dispersion parameters through analysis of concentration levels and the time it takes for the concentration levels to drop below preset values (e.g. Hanna and Franzese, 2000). However, depending on the height and point of sampling it may be difficult to obtain an accurate representation of the size of puffs. Lidar can be a valuable tool for obtaining measurements of the atmospheric state required for dispersion modelling. Recently, several studies have used lidar to estimate vertical dispersion parameters (Hiscox *et al*., 2005, 2006). The objective of this paper is to estimate horizontal and vertical dispersion parameters in an urban setting using lidar observations of puff spreading. From the dispersion parameters, eddy diffusivities can be estimated (required input for dispersion models such as LODI/ADAPT (Sugiyama *et al*., 2010 and DERMA (Danish Emergency Response Model of the Atmosphere, Sørensen, 1998)). Eddy diffusivities estimated by this approach are compared with values estimated from traditional approaches using sonic data.

The urban atmospheric boundary layer is markedly different from that over a rural area. This is primarily due to turbulence generated by enhanced roughness elements (buildings, bridges and other infrastructure) present in an urban area and also the altered thermal effects of the built environment (e.g. the urban heat island, Fernando, 2010). The spatially and temporally rich measurements provided by coherent Doppler lidar provide an opportunity to investigate complicated air motions in urban areas (Lin *et al*., 2008; Xia *et al*., 2008) and to verify theories on dispersal of pollutants. Using lidar it is possible to measure motions of puffs and plumes on the neighbourhood scale, providing an improved basis

* Correspondence to: A. Choukulkar, Environmental Remote Sensing Group, Arizona State University, Tempe Campus, PO Box 876106, Tempe, AZ 85287-6106, USA. E-mail: Aditya.Choukulkar@asu.edu

Figure 1. Geographical locations of ASU and ARL lidars along with the scanning regions and other instruments used in this study. This figure is available in colour online at wileyonlinelibrary.com/journal/met

for understanding exposures and human health effects associated with local effects in urban areas.

2. Experimental setup

The lidar data for this paper were acquired on the night of 4 July 2003, during the Joint Urban 2003 experiment (JU2003) in Oklahoma City which was conducted over a period of 34 days (from 28 June to 31 July 2003). The primary objectives were to characterize the urban boundary layer development and dispersion spanning a range of scales within and around building cores (Allwine and Flaherty, 2006). Two Doppler lidars were deployed (Figure 1): (1) The ASU lidar was positioned to the south-southeast of the urban core (or Central Business District – CBD) at a distance of approximately 3.8 km from the CBD, and, (2) the Army Research Laboratory (ARL) lidar was placed to the east of the CBD. Using the ASU lidar position as the origin, the location of the ARL lidar was approximately $Y = 3.96$ km and $X = -1.1$ km (north being the positive Y axis and west the negative X axis). Both lidars were approximately 380 m above mean sea level.

The ASU and ARL lidars performed a set of complementary scans to capture smoke puffs that were released into the atmosphere during the fireworks display on 4 July 2003 at 2100–2140 h LST (0300–0340 UTC). The ASU lidar performed a set of Plan Position Indicator (PPI) scans at elevation angles of 1° and 2.5° encompassing the CBD and ARL lidar. The ASU scans intersected the Range Height Indicator (RHI) scans of the ARL lidar, performed at azimuthal angles of approximately 208, 245 and 270° (measured clockwise from geographic north).

The Doppler lidars operated by Arizona State University and the Army Research Laboratory were of the WindTracer (2003) type (Lockheed Martin Coherent Technologies, Inc., 2003). The lidars use 2 μm, eye-safe, infrared laser beams to measure radial velocities of the wind field *via* Doppler shifts backscattered signals. The amount of laser light returned provides a measure of the backscatter from the aerosols present in each range-gate. Range-gates are the sensing volumes over which measurements are produced. The shape of the sensing volumes is cylindrical, approximately 10–30 cm in diameter and 50–80 m in length. The pulse repetition frequency is roughly 500 times *per* second.

The lidar has distinct differences compared to radar in terms of the accuracy and range of scales. Owing to the low divergence of the laser beam, side-lobe difficulties are avoided and high resolution measurements can be obtained close to the ground, only metres above with a typical range ∼5–10 km. The radial resolution is 50–100 m and the azimuthal resolution can be as low as a few metres depending on the angular speed of the scanner (configurable). During JU2003 the ASU lidar was scanning at 0.45° s^{-1} in the horizontal and the ARL lidar was scanning at 1° s^{-1} in the vertical.

3. Theoretical considerations

Owing to the complexity and diversity of flow conditions in the urban boundary layer, there can be a large variation in the rate of spreading for different puffs. The two main mechanisms of dispersion can be identified as turbulent diffusion, caused by mixing within the puff, and mean shear that is responsible for stretching and shearing of the puff (Richards, 1965). In the surface layer, the along-wind mean shear is usually greater than the directional shear (Hanna and Franzese, 2000) causing the puffs to be elongated in the x-direction (along-wind) than in the y-direction (cross-wind). The size of important turbulent motions (eddies) relative to the size of the puff affects the rate of dispersion. Eddies roughly equal to the size of the puff contribute dominantly to the growth of the puff. By contrast, eddies that are significantly larger than the size of the puff cause its advection (Hanna *et al*., 1982).

Therefore, dispersion occurs at two scales of motion: (1) due to turbulence scales close to and smaller than the cloud size (relative dispersion), and (2) on a much larger scale where turbulence acts on the whole cloud as a single entity (single particle diffusion or meander):

$$\sigma^2_{\text{total}} = \sigma^2_{\text{relative}} + \sigma^2_{\text{meander}} \tag{1}$$

where σ is the standard deviation of the puff concentration over an ensemble of puffs also referred to as the dispersion parameter. The present study focuses on measuring only the relative dispersion. That is, there is a cloud-following coordinate system with zero at the centre of the cloud and x – axis in the along wind direction. This results in $\sigma^2_{\text{meander}} = 0$, and therefore, $\sigma^2_{\text{total}} = \sigma^2_{\text{relative}}$ The vertical and horizontal (alongwind and cross-wind) concentration distribution in the puff can be estimated by fitting the puff concentration profile with a Gaussian curve of the form (Hiscox *et al.*, 2006):

$$C_{\text{e}} = C_{\text{m}} e^{-\Delta^2/2\sigma^2} \tag{2}$$

where C_{e} and C_{m} are the edge and maximum concentration values and Δ is the distance between the locations of maximum concentration to the location of the edge contour.

The dispersion parameter can be approximately obtained from the lidar backscatter values, B_{data} (e.g. Gifford, 1957; Min *et al.*, 2002). To do this, one must assume the concentration distribution in a puff is proportional to the backscatter values. Clearly, this is not strictly correct, although not unreasonable if the aerosol particles can be assumed to be spatially homogeneous in shape and constituency. Hence, let $C_{\text{e}} \propto B_{\text{e}}$ and $C_{\text{m}} \propto B_{\text{m}}$, where B_{e} represents the backscatter values on the edge of the puff contour and B_{m} the maximum backscatter value, the location of which is the centroid of the puff. The value of B_{e} is taken to be equal to the background backscatter level. The maximum backscatter intensity level can be defined as $\Delta B = B_{\text{m}} - B_{\text{e}}$ in the x, y and z directions. The actual concentrations can be replaced with the backscatter values in Equation (2). This expression needs to be offset by the background backscatter value (B_{e}), as the lidar measures non-zero residual backscatter returns from the dust and trace aerosols present outside the puff. Thus, the expressions for the backscatter distributions can be written as follows:

$$B(x)_x = \Delta B_x e^{-\Delta_x^2/2\sigma_x^2} + B_{ex} \tag{3}$$

$$B(y)_y = \Delta B_y e^{-\Delta_y^2/2\sigma_y^2} + B_{ey} \tag{4}$$

$$B(z)_z = \Delta B_z e^{-\Delta_z^2/2\sigma_z^2} + B_{ez} \tag{5}$$

where subscripts x, y and z signify the along wind, cross wind and vertical cross sections, respectively, B_{ex}, B_{ey}, and B_{ez} are the base of the Gaussian profiles, B_{m} is the value at the peak and ΔB_x, ΔB_y and ΔB_z are the amplitudes of the Gaussian peaks.

The dispersion parameter σ_x is determined by minimizing the mean square error E_x between the estimated backscatter values obtained from the lidar data, $B_{\text{data}}(x)$, and the model predictions $B(x)_x$. σ_y and σ_z can be similarly defined:

$$E_x = \frac{1}{N_x}\sum_{k=1}^{N_z}[B_{\text{data}}(x) - B(x)_x]^2 \tag{6}$$

$$E_y = \frac{1}{N_y}\sum_{k=1}^{N_z}[B_{\text{data}}(y) - B(y)_y]^2 \tag{7}$$

$$E_z = \frac{1}{N_z}\sum_{k=1}^{N_z}[B_{\text{data}}(z) - B(z)_z]^2 \tag{8}$$

where N_x, N_y and N_z are the number of data points.

The standard deviation of the puff concentration (or the dispersion parameter σ_x, σ_y, or σ_z, which is equal to the standard deviation of the backscatter fitted curve) is the value which gives the least error between the actual backscatter values and the model predictions. Thereafter, the following relationships can be used from the gradient transport theory to calculate the eddy diffusivities K_x, K_y and K_z:

$$\sigma_x = (2K_x t)^{1/2} \quad \sigma_y = (2K_y t)^{1/2}$$
$$\sigma_z = (2K_z t)^{1/2} \tag{9}$$

$$K_x = \frac{1}{2}\frac{d\sigma_x^2}{dt} \quad K_y = \frac{1}{2}\frac{d\sigma_y^2}{dt} \quad K_z = \frac{1}{2}\frac{d\sigma_z^2}{dt} \tag{10}$$

The puffs are considered non-buoyant as considerable time is believed to have been elapsed since their release. The buoyancy effects can be assumed to be negligible due to the fact that the puff height does not seem to change much. This is inferred from the fact that the scan is nearly horizontal (2.5° elevation angle) and the puff does not leave the line of sight of the lidar.

In order to validate the results obtained from the above analysis, an alternative, independent, method of estimating the eddy diffusivity can be used to establish confidence. To this end, a complementary method based on similarity theory is given below. As mentioned above, it has been observed in the surface layer that dispersion is greater in the along-wind than the cross-wind direction (Hanna and Franzese, 2000), which is consistent with the observed oblong shape of puffs in the backscatter data. The inspection of governing variables indicates that the friction velocity, the time after release, mixing height, surface roughness and the Monin-Obukhov length are important parameters governing the rate of puff dispersion. Most of these parameters are dependent of the state of the atmosphere and its stability.

The state of the atmosphere at the time of observations was evaluated using temperature data obtained from the rawindsonde operated by the Army Research Laboratory (ARL). See Figure 2 for 1 h averaged potential temperature profiles between 2000 and 2200 LST.

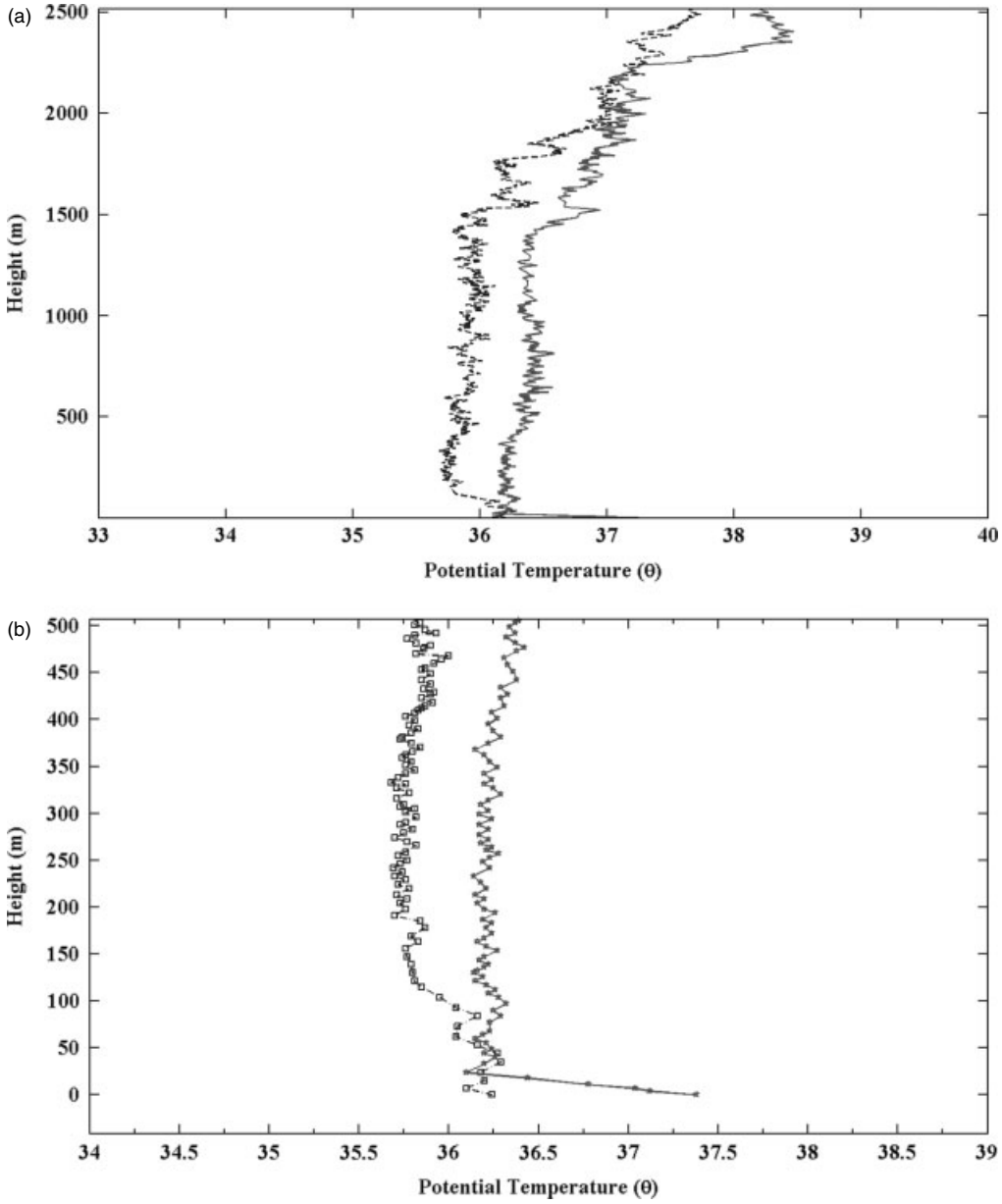

Figure 2. Potential temperature profiles on 4 July, 2003 at 2100 and 2200 h local time (0200 and 0300 UTC). (a) Temperature profiles till a height of 2500 m. The solid line and the dashed line are potential temperatures at 2100 h and 2200 h local time. (b) Temperature profiles for the first 500 m. The points represented by the squares and the stars are potential temperatures at 2100 h and 2200 h local time.

Therein the stability is mostly neutral till about 2000 m and then becomes stable. Neutral regimes are not uncommon in urban areas even at night due to the additional upward heat flux caused by the urban heat island effect (Barrat, 2001; Britter and Hanna, 2003). All the puffs observed were below 200 m and hence were in the neutral boundary layer. The surface layer height is approximately 200 m and is consistent with that reported by Simpson *et al*. (2006). Data obtained from the sonic anemometers set up by the Lawrence Livermore National Laboratory (LLNL) are used for this analysis. The sonic anemometer crane allows measurements at heights of 21.5, 28.3, 42.5, 55.8, 69.7 and 83.2 m above ground level. Data gathered from 69.7 and 83.2 m are used in the calculations. For the temperature profiles, data from the Argonne National Laboratory (ANL) profiler/RASS were used.

In a near neutral boundary layer, puff releases in the surface layer obey the following relation for the along-wind dispersion coefficient (Chatwin, 1968):

$$\sigma_x = Du_* t \tag{11}$$

where the constant D is estimated to be somewhere between 1 and 3 (and is found by fitting to data), u_* is the friction velocity, and t is the time since release of the puff. In addition, puffs in the surface layer are affected by the wind shear present causing them to be elongated in the along-wind direction (see Figures 3–8). The dispersion mechanism responsible for these effects

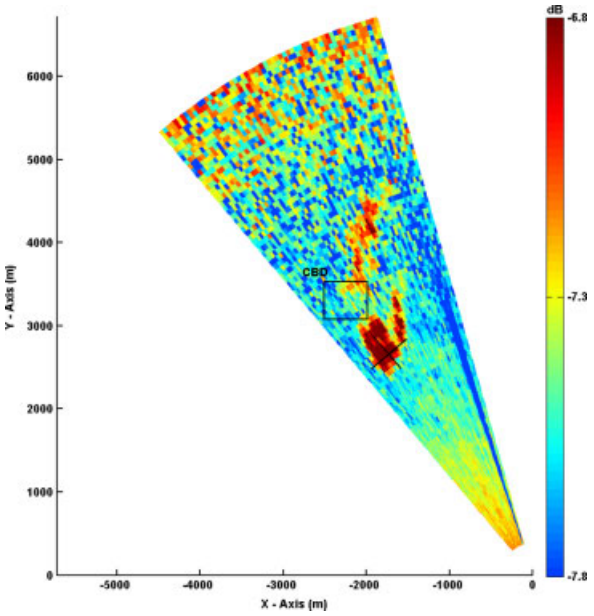

Figure 3. Lidar image of the puff captured on the night of 4 July 2003 at 213 822 LST - t0, (033 822 UTC) and elevation angle of 2.5° as it moves into the field of the lidar. This figure is available in colour online at wileyonlinelibrary.com/journal/met

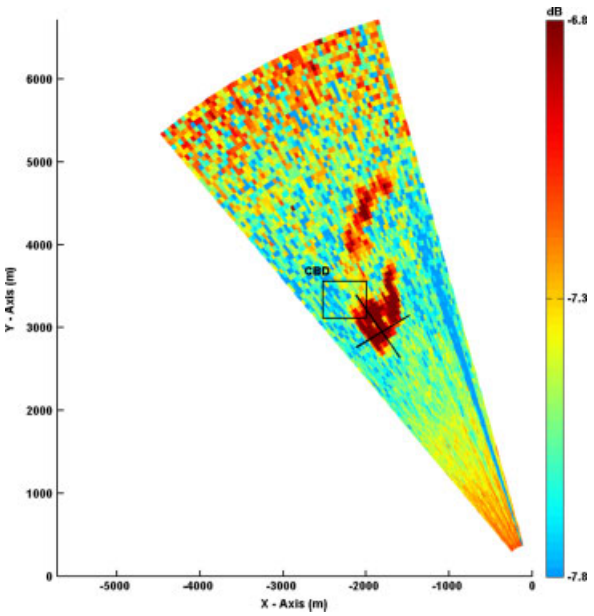

Figure 4. Lidar image of the puff captured on the night of 4 July 2003 at 213 848 LST - t0+26 sec, (033 848 UTC) and elevation angle of 2.5°. This figure is available in colour online at wileyonlinelibrary.com/journal/met

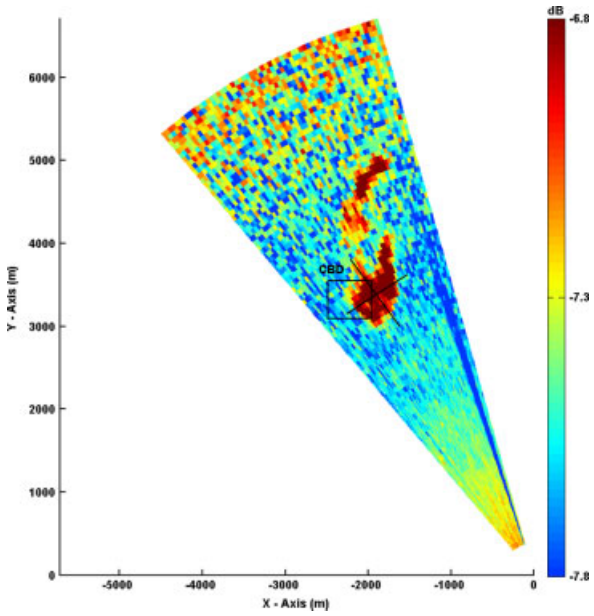

Figure 5. Lidar image of the puff captured on the night of 4 July 2003 at 213 914 LST - t0+52 sec, (033 914 UTC) and elevation angle of 2.5°. This figure is available in colour online at wileyonlinelibrary.com/journal/met

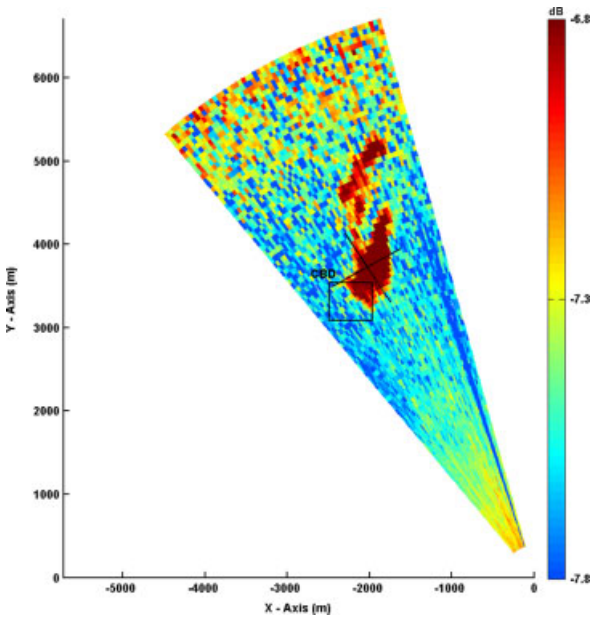

Figure 6. Lidar image of the puff captured on the night of 4 July 2003 at 213 940 LST - t0+78 sec, (033 940 UTC) and elevation angle of 2.5°. This figure is available in colour online at wileyonlinelibrary.com/journal/met

was studied by van Ulden (1992) and developed the following parameterization for eddy diffusivity:

$$K_x = \alpha \sigma_x \sigma_u \tag{12}$$

where α is an empirical constant with a value of 0.3, σ_x is the dispersion coefficient in the along wind direction, and σ_u is the standard deviation of the wind fluctuations in the along wind direction.

A similar parameterization for the lateral spread was given by Heffter (1965) as:

$$\sigma_y = 0.5 \times t \tag{13}$$

This parameterization was found to be a good fit for travel distances of 30 m to 200 km and travel times of 30 s to 4 days. As given previously for the x - direction, the eddy diffusivity is then related to

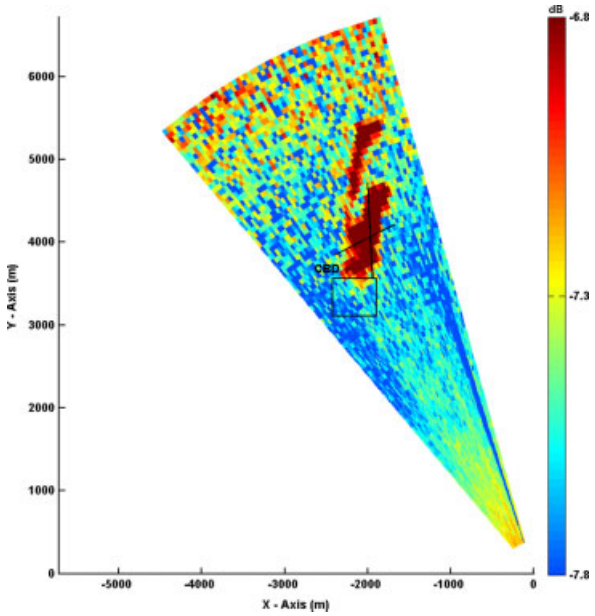

Figure 7. Lidar image of the puff captured on the night of 4 July 2003 at 214 006 LST - t0+104 sec, (034 006 UTC) and elevation angle of 2.5°. This figure is available in colour online at wileyonlinelibrary.com/journal/met

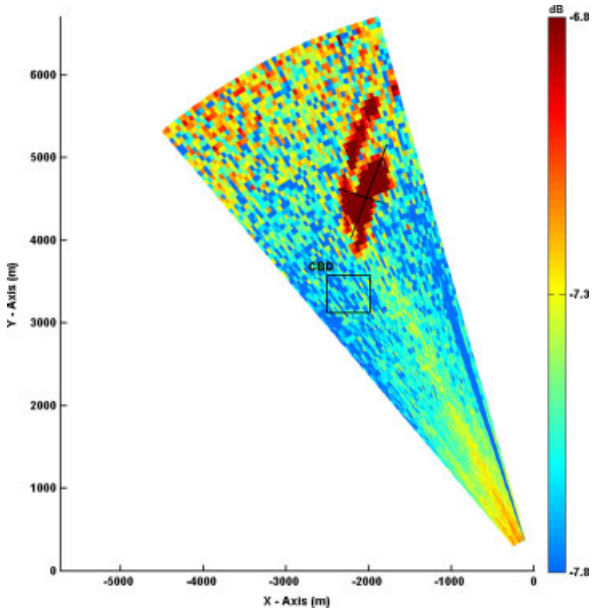

Figure 8. Lidar image of the puff captured on the night of 4 July 2003 at 214 032 LST - t0+130 sec, (034 032 UTC) and elevation angle of 2.5°. This figure is available in colour online at wileyonlinelibrary.com/journal/met

the dispersion with the following parameterization (van Ulden, 1992):

$$K_y = \alpha \sigma_y \sigma_v \tag{14}$$

For the vertical eddy diffusivity, the following semi-empirical formulation was used, assuming the applicability of Monin–Obukhov (MO) theory (Dyer, 1974; Jensen *et al.*, 1984):

$$K_z = k u_* z / \phi_h(z/L) \tag{15}$$

where $k = 0.4$ is the von Karman constant, u_* is the friction velocity, L is the MO length and,

$$\phi_h(z/L) = (1 - 16z/L)^{-1/2} \quad for \quad L \leq 0, \tag{16}$$

$$\phi_h(z/L) = 1 + 5z/L \quad for \quad L \geq 0. \tag{17}$$

The friction velocity (u_*) and the MO length (L) required in the above equations are calculated from the sonic anemometer data. The following formulations are used to calculate the friction velocity and the MO length:

$$u_* = (-\overline{u'\ w'})^{1/2} \tag{18}$$

$$L = -u_*^3 T\ \rho C_P / (0.4 g Q_H) \tag{19}$$

$$Q_H = C_P \rho \overline{w'T'} \tag{20}$$

where C_P is the specific heat of air at constant pressure, T is the temperature of air, ρ is the density of air, and w' is z-direction (vertical) velocity fluctuation. To the first order, the similarity relations above are assumed applicable to the urban surface layer; note that the observations are made at sufficient height that the constant flux layer assumption underlying the MO similarity is valid (Fernando, 2010) The average building height of the area was about 60 m, and hence the constant flux layer is expected to exist beyond about 120 m.

4. Results and observations

On the night of 4 July during the fireworks display between 2100 to 2140 LST, the ASU lidar and the ARL lidar captured the puffs of smoke generated as they advect into the line of sight of the lidar at about 2138 LST. The puffs are assumed to be passive and non-buoyant as considerable time is elapsed before they are captured by the lidar. Also, the puffs do not show a significant rise in altitude as they stay in the line of sight of the lidar which is almost horizontal (2.5° elevation angle). The ASU lidar measured the puff at six instances (see Figures 3–8) while the ARL lidar captured it at three. The images captured by the ASU and ARL lidars are shown in Figure 9 (approximately 2139 LST). From these backscatter data it is possible to calculate the dispersion parameter (σ) of the puff using Equations (3)–(5). In using Equations (6)–(8), an initial guess of the dispersion parameter in each of the directions ($\sigma_x, \sigma_y, \sigma_z$) is required, and half of the puff size was used as the initial guess.

The dispersion in the vertical direction was captured by the RHI scans of the ARL lidar. These RHI scans intersect the PPI scans from the ASU lidar, but they do not capture the puff at exactly the same instant. There was a maximum time lag of 13 s, which was relatively small and thus the puff images can be assumed as captured instantaneously. The intersection of the scans occurred very close to the puff centre line, and the dispersion parameters calculated should be close to the actual σ values.

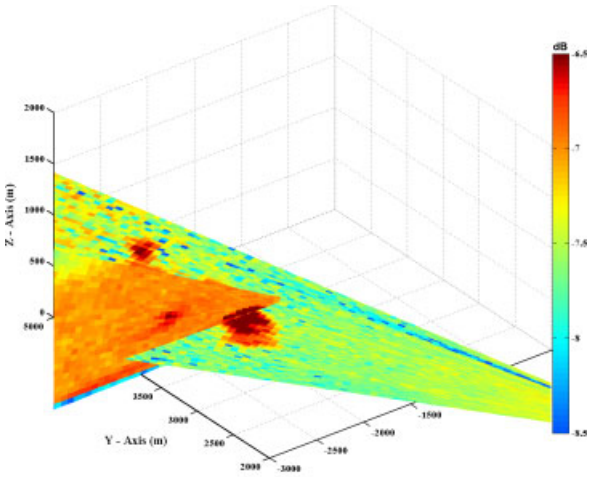

Figure 9. Intersection of a RHI and PPI scan on a puff at times 213 940 LST (033 940 UTC) for the ASU lidar scan at elevation 2.5° and 213 921 LST (033 921 UTC) for the ARL lidar scan at an azimuthal angle of 245°. This figure is available in colour online at wileyonlinelibrary.com/journal/met

The location from where the backscatter is taken is indicated with black solid lines on the PPI scans shown in Figures 3–8, and the estimated dispersion parameter is used to plot the model Gaussian backscatter distribution over the actual observed backscatter values. An example case for all three directions is shown in Figures 10–12. Note that there is reasonable agreement between the actual backscatter values retrieved from the lidar scans and the Gaussian fit, supporting the initial assumption that the concentration distribution can be approximated in this manner.

The same analysis is carried out at all the six instances where the puff was captured by the ASU lidar. The backscatter values are plotted for this same puff in the along wind and crosswind direction at each location. To plot the backscatter in the vertical direction, RHI scans are needed that intersect the PPI scans at the puff locations, and in the present data set this occurred for three instances.

The ratio σ_x/σ_y is initially 0.75 and then increases to 1.15, confirming higher dispersion in the along wind direction than in the cross-wind direction. The ratio σ_y/σ_z varies from 4 to 7, suggesting the possibility of a local inversion inhibiting vertical spread of the aerosol, although there is no further evidence as yet for this conjecture (except that, as shown in Figure 2, local inversions are common in these profiles).

Once the dispersion parameters are estimated, the eddy diffusivities can be calculated using Equations (9) and (10). Diffusivities so estimated are plotted in Figures 13–15. The average values of K_x, K_y, and K_z calculated from this method are 95.46, 175.7 and 17.46 m^2 s^{-1}, respectively. As noted earlier, the eddy diffusivity in the z-direction can be estimated for only two instances and was found to be 31.4 and 3.52 m^2 s^{-1}. The variability observed is large, but not uncommon (Arya, 1999). More data would be required before making definitive conclusions for the eddy diffusivity values in this scenario.

In order to validate the results obtained using the Gaussian model, the similarity relations can be used (Section 3). Equations (11)–(20) are used to estimate the eddy diffusivities. The diffusivities so calculated are presented in Figures 16–18. It can be seen that the results from the two techniques are consistent except for the diffusivity in the z-direction. The average values of the diffusivity in the z-direction calculated from the lidar measurements was 17.45 m^2 s^{-1}, vis-à-vis 89.23 m^2 s^{-1} obtained by the similarity formulation (puff height at this location was 150 m). One possible cause for the difference could be that the lidar backscatter curve-fit (Gaussian) method is accurately reflecting low diffusivity in the vertical, as is evidenced by the thinness of the puffs in the vertical, while the similarity method is unable to represent accurately the narrow vertical layering that limits the vertical dispersion. It could be possible there are locally

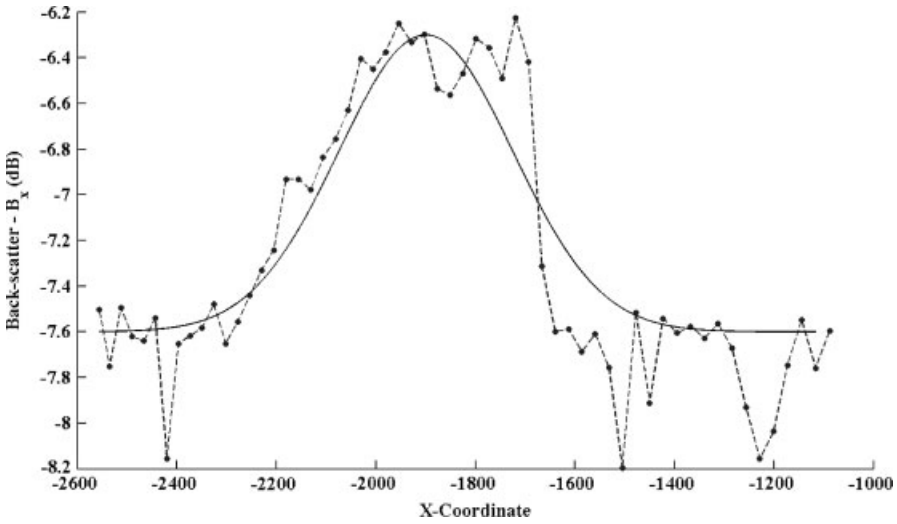

Figure 10. Lidar-measured backscatter and Gaussian fitted curve versus the along-wind direction (x). The dashed line is the backscatter from lidar data and the solid line is the Gaussian fit.

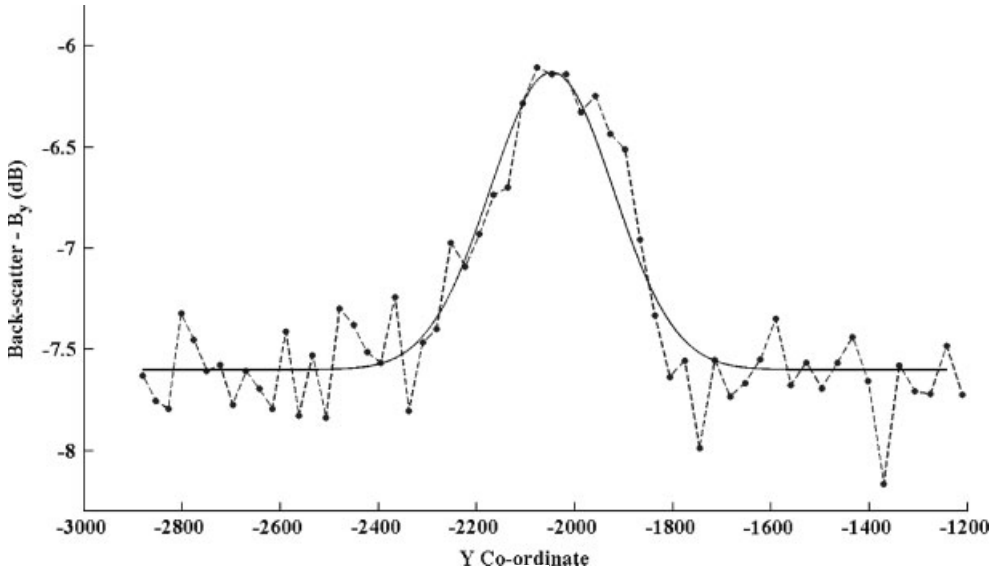

Figure 11. Backscatter plotted in comparison with the Gaussian fitted curve along the horizontal cross-wind (y) direction. The dashed line is the backscatter from lidar data and the solid line is the Gaussian fit.

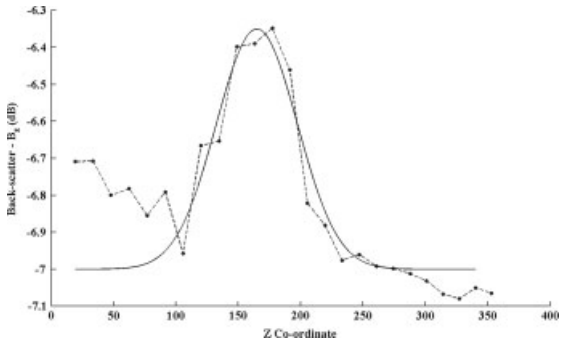

Figure 12. Backscatter values plotted in comparison with the Gaussian fitted curve in the vertical cross-wind (z) direction. The dashed line is the backscatter from lidar data and the solid line is the Gaussian fit.

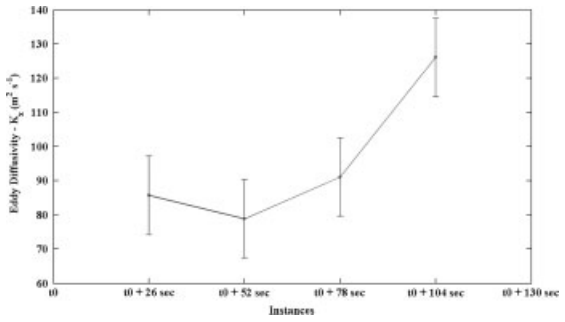

Figure 13. Eddy Diffusivities in the x – direction (along wind).

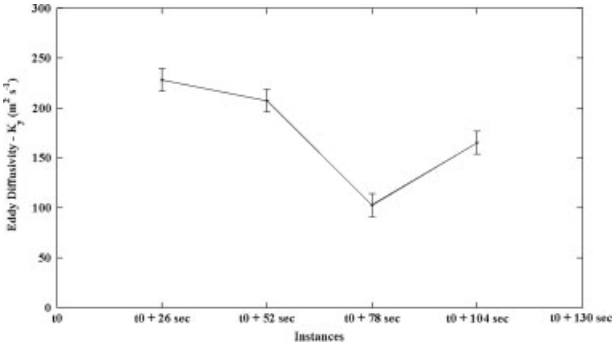

Figure 14. Eddy Diffusivities in the y – direction (cross wind).

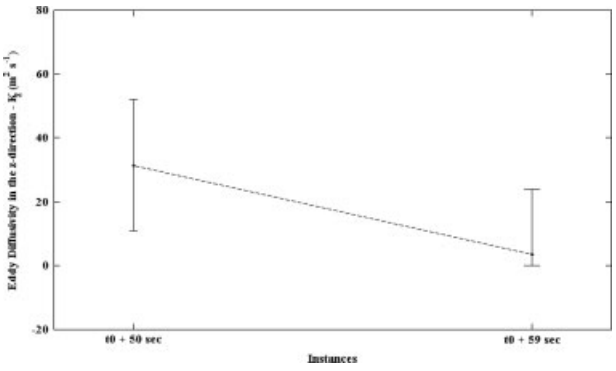

Figure 15. Eddy Diffusivity in the z – direction (vertical).

stratified layers present that are inhibiting vertical dispersion, but there seems to be no concrete evidence of presence of such layers at this point and further study is required. Alternatively, RHI scans may not be intersecting the puff at the same place every time. If one scan intersects the puff near its centre, but the next intersects the puff too far from the centre, this could lead to an underestimation of eddy diffusivity. Tirabassi and Rizza (1997) calculated eddy diffusivities in the vertical using K theory with truncated Gram-Charlier expansions and found values ranging from 20 to 100 m^2 s^{-1} depending on the method and the dataset used. Horizontal eddy diffusivity values of around 50 m^2 s^{-1} are typical in urban areas (Arya, 1999). Therefore, the values obtained here vary by a factor of 2–3 when compared to these studies. This kind of disagreement is common as can be

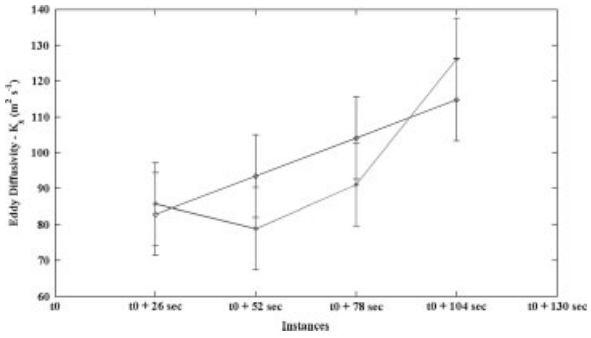

Figure 16. Comparison of eddy diffusivities in the x – direction (along wind). Points represented by asterix (*) are values calculated from lidar data, while circles are values calculated from similarity theory.

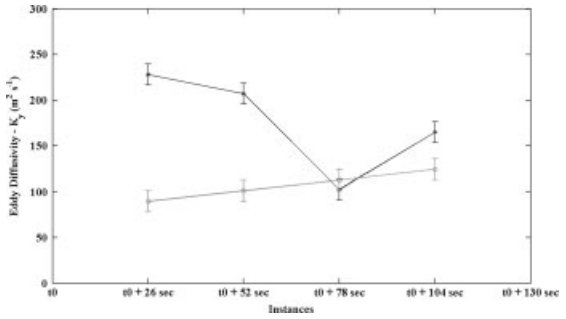

Figure 17. Comparison of eddy diffusivities in the y – direction (cross wind). Points represented by asterix (*) are values calculated from lidar data, while circles are values calculated from similarity theory.

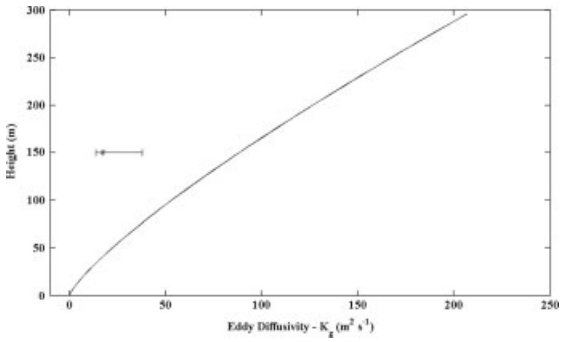

Figure 18. Comparison of eddy diffusivities in the z – direction (vertical). Solid line is result from similarity theory and asterix (*) is result from the lidar data.

seen in the values calculated by Tirabassi and Rizza (1997).

As discussed previously, more extensive and well planned experimentation is required for accurate characterization of the dispersion process. The purpose here is to assemble, develop and demonstrate the methodology used to retrieve dispersion parameters from Doppler lidar data in a plume/puff tracking experiment. Further refinement in the experimental setup would involve having multiple aerosol releases from the southwest of the CBD and performing more closely spaced scans with the lidars. As examples of suggested scanning improvements in this scenario: (1) the ASU lidar could have performed scans from elevation angles of 1 to 2.5° in steps on 0.5° (with the current azimuth range of 320 to 344° clockwise from north), and, (2) while the ARL lidar could have performed intersecting RHI scans (with current elevation range of 0–30° from the horizontal) at 210, 220, 230, 240, 245, 250, 260 and 270° azimuth measured clockwise from north. This would have ensured that a larger number of instances of the puffs would have been captured over the CBD.

5. Conclusions

This study demonstrated an approach for the use of Doppler lidar data to retrieve dispersion characteristics of an urban nocturnal boundary layer. It was shown that Doppler lidar is an effective tool for dispersion analysis, e.g. tracking the evolution of puffs and educing dispersion parameters in both the horizontal and vertical directions. The dispersion parameters for the puff and the eddy diffusivities were calculated using the Gaussian model, as well as, the similarity relations, and the results from both these analyses showed reasonable agreement given the limits of our dataset. It should be noted that in this analysis it is assumed that the lidar scans intersect the puffs along its central axis and that the true size of the puff is being captured. The only way to ensure this would be through using tightly spaced scans as explained above. In addition, the effects of vertical shear are not considered in this analysis.

While the JU2003 experiment provided a serendipitous opportunity to analyze smoke puffs directly with Doppler lidar, a refined experiment obtaining a more extensive dataset is suggested to further verify and extend the above methods. The aim of this work was to develop the foundation for lidar-informed dispersion modelling by demonstrating methods for the estimation of key inputs (such as dispersion parameters, eddy diffusivities, friction velocities and Monin-Obukhov lengths). Owing to the complexity of the relationships between eddy diffusivities and boundary layer parameters, lidar-informed estimation of dispersion model inputs would seem especially valuable, providing a way for models to adapt to changing and complex atmospheric conditions.

Acknowledgements

The ASU lidar group would like to recognize the support of the Army Research Office for their sponsorship (grant W911NF-04-1-0146, Project Officer: Dr. Walter Bach) that made this work possible. The lidar group would also like to thank the Army Research Laboratory (ARL) and the Argonne National Laboratory (ANL) and the Lawrence Livermore National Laboratory (LLNL) for the use of their data that was crucial for the present analysis.

References

Allwine KJ, Flaherty JE. 2006. Joint Urban 2003: study overview and instrument locations. PNNL-15967, Pacific Northwest National Laboratory: Richland, WA; 92 pp.

Arya SP. 1999. *Air Pollution Meteorology and Dispersion*. Oxford Press: New York, NY.

Barrat R. 2001. *Atmospheric Dispersion Modelling: An Introduction to Practical Applications*. Earthscan Publications Limited: Sterling, VA.

Britter RE, Hanna SR. 2003. Flow and dispersion in urban areas. *Annual Review of Fluid Mechanics* **35**: 469–496.

Chatwin PC. 1968. The dispersion of a puff of passive contaminant in the constant stress region. *Quarterly Journal of the Royal Meteorological Society* **94**: 350–360.

Collier CG, Davies F, Bozier KE, Holt AR, Middleton DR, Pearson GN, Siemen S, Willetts DV, Upton GJ, Young RI. 2005. Dual-Doppler lidar measurement for improving dispersion models. *Bulletin of the American Meteorological Society* **86**: 825–838.

Dyer AJ. 1974. A review of the flux profile relationships. *Boundary Layer Meteorology* **7**: 363–372.

Fernando HJS. 2010. Fluid dynamics of urban atmospheres in complex terrain. *Annual Reviews of Fluid Mechanics* **42**: 365–389.

Gifford FA. 1957. Relative atmospheric diffusion of smoke puffs. *Journal of Meteorology* **14**: 410–414.

Hanna SR, Briggs GA, Hosker RP Jr. 1982. *Handbook on Atmospheric Dispersion*, DOE/TIC-11223. Technical Information Centre, U.S. Department of Energy: Oak Ridge, TN.

Hanna SR, Franzese P. 2000. Alongwind dispersion – a simple similarity formula compared with observations at 11 field sites and in one wind tunnel. *American Meteorological Society* **39**: 1700–1714.

Hanna SR, Paine RJ. 1989. Hybrid plume dispersion model (HPDM) development and evaluation. *American Meteorological Society* **28**: 206–224.

Heffter JJ. 1965. The variation of horizontal diffusion patterns with time for travel periods of one hour or longer. *Journal of Applied Meteorology* **4**: 153–160.

Hiscox AL, Miller DR, Nappo CJ, Ross J. 2006. Dispersion of fine spray from aerial applications in stable atmospheric conditions. *American Society of Agricultural and Biological Engineers* **49**: 1513–1520.

Hiscox AL, Nappo CJ, Miller DR. 2005. On the use of lidar images of smoke plumes to measure dispersion parameters in the stable boundary layer: notes and correspondence. *Journal of Atmospheric and Oceanic Technology* **23**: 1150–1154.

Jensen NO, Petersen EL, Toren I. 1984. Extrapolation of mean wind statistics with special regard to wind energy applications. World Climate Program Report No WCP-86, WMO: Geneva; 85 pp.

Lin C, Xia Q, Calhoun R. 2008. Retrieval of urban boundary layer structures from Doppler lidar data. Part II: Proper orthogonal decomposition. *Journal of the Atmospheric Sciences* **65**: 1, 21–42.

Lockheed Martin Coherent Technologies. 2003. *Wind Tracer System Operation User Manual*. Louisville, CO.

Min IA, Abernathy RN, Lundblad HL. 2002. Measurement and analysis of puff dispersion above the atmospheric boundary layer using quantitative imagery. *American Meteorological Society* **41**: 1027–1041.

Misra PK, McMillan AC. 1980. On the dispersion parameters of plumes from tall stacks in a shoreline environment. *Boundary-Layer Meteorology* **19**: 175–185.

Richards JM. 1965. Puff motions in unstratified surroundings. *Journal of Fluid Mechanics* **21**: 97–106.

Savov PB, Sakakalova TS, Kolev IN. 2002. Lidar investigation of the temporal and spatial distribution of atmospheric aerosols in mountain valleys. *Journal Applied Meteorology* **41**: 528–541.

Simpson M, Raman S, Lundquist JK, Leach M. 2006. A study of the variation of urban mixed layer heights. *Atmospheric Environment* **41**: 6923–6930.

Sørensen JH. 1998. Sensitivity of the DERMA long-range Gaussian dispersion model to meteorological input and diffusion parameters. *Atmospheric Environment* **32**: 4195–4206.

Sugiyama G, Chan ST, Maddix D, Nasstrom J, Prevost L. 2001. *ADAPT (Atmospheric Data Assimilation and Parameterization Techniques)*. Lawrence Livermore National Laboratory: Livermore, CA.

Tirabassi T, Rizza U. 1997. Boundary layer parameterization for a non-Gaussian puff model. *Journal of Applied Meteorology* **36**: 1031–1037.

van Ulden AP. 1992. A surface layer similarity model for the dispersion of a skewed passive puff near the ground. *Atmospheric Environment* **26A**(4): 681–692.

Van Aalst RM. 1990. Atmospheric dispersion modelling for emergency response. *Meteorological Aspects of Emergency Response*. American Meteorological Society: Boston, MA; 57 pp.

Xia Q, Lin C, Calhoun R, Newsom R. 2008. Retrieval of urban boundary layer structures from Doppler lidar data. Part I: Accuracy assessment. *Journal of the Atmospheric Sciences* **65**(1): 3–20.

